



Synergy between silk fibroin and ionic liquids for active gas-sensing materials



Inês P. Moreira^{a,b}, Carina Esteves^{a,b}, Susana I.C.J. Palma^{a,b}, Efthymia Ramou^{a,b}, Ana L.M. Carvalho^{a,b}, Ana C.A. Roque^{a,b,*}

^a Associate Laboratory i4HB - Institute for Health and Bioeconomy, NOVA School of Science and Technology, NOVA University of Lisbon, 2829-516, Caparica, Portugal

^b UCIBIO – Applied Molecular Biosciences Unit, Department of Chemistry, NOVA School of Science and Technology, NOVA University of Lisbon, 2829-516, Caparica, Portugal

ARTICLE INFO

Keywords:

Silk fibroin
Ionic liquids
Physical ionogels
Ionic conductivity
Bioelectronics
Gas sensing

ABSTRACT

Silk fibroin is a biobased material with excellent biocompatibility and mechanical properties, but its use in bioelectronics is hampered by the difficult dissolution and low intrinsic conductivity. Some ionic liquids are known to dissolve fibroin but removed after fibroin processing. However, ionic liquids and fibroin can cooperatively give rise to functional materials, and there are untapped opportunities in this combination. The dissolution of fibroin, followed by gelation, in designer ionic liquids from the imidazolium chloride family with varied alkyl chain lengths (2–10 carbons) is shown here. The alkyl chain length of the anion has a large impact on fibroin secondary structure which adopts unconventional arrangements, yielding robust gels with distinct hierarchical organization. Furthermore, and due to their remarkable air-stability and ionic conductivity, fibroin ionogels are exploited as active electrical gas sensors in an electronic nose revealing the unravelled possibilities of fibroin in soft and flexible electronics.

1. Introduction

The natural polymer silk from *Bombyx mori* silkworm has a long history in the textile industry and biomedical field due to the unique biodegradability and biocompatibility allied to excellent mechanical properties. These features recently triggered the interest for silk-fibroin based materials in bioelectronics for wearable and flexible devices, albeit still hampered by the limited dissolution of fibroin and by the lack of fibroin-intrinsic conductive properties [1,2].

Silk fibroin, the constituent fibrous protein in the silk fibre core, has a repetitive hexameric motif in its primary structure (Gly-Ala-Gly-Ala-Gly-Ser), with short side chain units closely packed in hydrophobic crystalline regions due to extensive hydrogen bonds. This singular composition contributes to the excellent mechanical properties but also explains the limited solubility in water. In fact, the dissolution and further regeneration of silk fibroin are two challenging steps for which several solvents have been assessed. As an alternative to harsh solvents or aqueous inorganic salts, ionic liquids (ILs) have appeared as effective molecular solvents for the dissolution and regeneration of silk fibroin, exempting subsequent dialysis and significantly reducing the steps of fibroin

regeneration [3,4]. ILs are organic salts considered designer solvents due to the versatility in combining anions and cations. Both cation and anion moieties in ILs play an important role in silk fibroin dissolution. After dissolution, the secondary structure of silk fibroin can be altered and transformed back into a water-insoluble structure using coagulation solvents (ethanol, methanol [5], water [6] or even protic ILs [7]). After fibroin regeneration and IL removal, hydrogels [8], films [9] or other materials are produced for different applications. As such, ILs have been so far regarded as silk fibroin dissolution and regeneration agents, which are not present (or only partially) in the final fibroin assembled materials [10,11].

Ionogels are generated when ILs are physically entrapped in gelators, such as polymeric matrices. The properties of ILs are typically transferred to the derived ionogels, namely air-stability and ionic conductivity, making ionogels excellent candidates to yield electronic devices [12]. The research on silk fibroin for flexible electronics and sensing has been so far focused on its use as a substrate [2] and not as an active component. Composite fibroin materials for use in electronics are obtained by incorporating conducting moieties, namely polymers (e.g. polypyrrole [13]) and nanomaterials (e.g. carbon nanotubes [14], silver nanowires

* Corresponding author.

E-mail address: cecilia.roque@fct.unl.pt (A.C.A. Roque).

<https://doi.org/10.1016/j.mtbio.2022.100290>

Received 7 April 2022; Received in revised form 10 May 2022; Accepted 11 May 2022

Available online 16 May 2022

2590-0064/© 2022 The Authors. Published by Elsevier Ltd. This is an open access article under the CC BY-NC-ND license (<http://creativecommons.org/licenses/by-nc-nd/4.0/>).

[15] or gold nanoparticles [16]) into silk fibroin. As an alternative to ILs, ionotronic materials using metal ions and water, are also interesting options to generate silk fibroin conducting materials [17].

Despite the possible synergetic properties of silk fibroin and ILs, the full potential of this combination for advanced functional materials has not been met. In the present work, the possibility to use fibroin as an ionogelator of methylimidazolium chloride ILs, in the absence of water, was assessed yielding soft materials with unique tunable supramolecular architectures. Furthermore, the resultant air-stable and ionic-conductive fibroin ionogels were assessed as active gas sensing layers for artificial olfaction, widening the impact and applicability of silk fibroin in flexible and wearable bioelectronics and non-invasive sensing devices.

2. Materials and methods

2.1. Materials

Silk fibroin solution (50 mg mL⁻¹) was purchased from Advanced BioMatrix, which is a partially hydrolysed silk fibroin II solution, harvested from domesticated *Bombyx mori*. The ionic liquids 1-Ethyl-3-methylimidazolium chloride >98% (C₂mimCl), 1-Hexyl-3-methylimidazolium chloride 99% (C₆mimCl) and 1-Decyl-3-methylimidazolium chloride >98% (C₁₀mimCl) were purchased from Iolitec (Germany) and used as supplied.

2.2. Preparation and characterisation of fibroin ionogels

The 50 mg mL⁻¹ fibroin solution was lyophilised, resulting in a water insoluble lyophilised fibroin sample. Fibroin ionogels were prepared by stirring each ionic liquid at 70 °C, and slowly adding the lyophilised fibroin up to 100 mg mL⁻¹ or 8.76% w/w (check Supplementary Methods and Table 1 for details). The vial was then placed at room temperature after full fibroin dissolution and gelation occurred immediately without any further action. Nomenclature for the fibroin ionogels developed in this work is C_nF, with n representing the number of carbons in the IL methylimidazolium cation alkyl chain and F the fibroin presence, as depicted in Table 1. Control samples of heat/cooled ionic liquids were prepared following a similar procedure, except without fibroin addition, and they are labelled C_nHC, with n representing the number of carbons in the IL alkyl chain and HC the heat/cool cycle they are subjected to. The control fibroin hydrogel was prepared by pipetting the commercial fibroin solution (50 mg mL⁻¹) into a vial and vortex stirring it at maximum speed in an upright position until the solution became turbid (5/7 min depending on the volume), as described in the supplier's usage indications. In some cases, the vial was then placed in a 37 °C incubator overnight to decrease gelation time.

Details on equipment and samples' preparation for morphological (atomic force microscopy, transmission electron microscopy, polarised optical microscopy), mechanical and structural characterisation (rheology, ATR-FTIR, X-ray scattering), as well as air stability, thermal and conducting properties (stability to storage, DSC, thermal investigations, ionic conductivity) of fibroin ionogels can be found on the Supplementary Methods of Supplementary data. Ionogel samples were left to stand at room temperature and 50% relative humidity for at least

24 h before being characterised (as detailed in Supplementary Information, unless otherwise stated).

2.3. Preparation of fibroin ionogel thin films

15 µL of each sample were spread into films on top of Gold-Titanium interdigitated electrodes deposited on untreated glass substrates (18 parallel, 300 µm in width, spaced by 300 µm). This was carried out using an automatic film applicator with a heated bed and a quadruplex with a predefined thickness of 15 µm (TQC, The Netherlands). All films were left to stand at room temperature and 50% relative humidity for at least 24 h before being used for sensing purposes.

2.4. VOC sensing using fibroin ionogel thin films

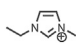
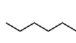
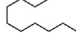
The fibroin ionogel thin films were placed in the chamber of an in-house tailor-made electronic nose [18]. The sensors were exposed to a sequence set of 10 volatile organic compounds (VOCs) from different chemical classes, following an order of increased polarity (Table S1), and finishing with water. Pure solvents were heated up to 37 °C for 15 min and the resulting vapours in the headspace of the sample vial were pumped through the sensors, using cycles of 5 s exposure to VOC and 15 s recovery with ambient air, for a total of 7.5 min (22 consecutive cycles). Electrical signals were acquired at a sampling rate of 90 Hz. Different batches of films were produced so that duplicates were analysed and reproducibility was assured. The conductance of the sensing materials (the electrical signal) was independently analysed using computing processes and machine learning tools. Signals were first filtered using a median filter from the signal processing (scipy.signal) Python library and a smooth filter from novainstrumentation Python library (<https://github.com/hgamboa/novainstrumentation>), and divided in cycles. To analyse sensors' repeatability and reproducibility, the relative signal, average and standard deviation of cycles were calculated. The relative signal (Sr) for each cycle was calculated according to the equation

$$Sr = \frac{S - \text{baseline}}{\text{baseline}}$$

where *S* is the filtered cycle signal and *baseline* is the average of the filtered cycle signal taken from 10 points immediately before VOC exposure. The maximum variability of a cycle was estimated as the ratio between the maximum standard deviation and the average cycle signal taken over 15 to 20 cycles. To assess the ability of each sensing material to identify VOCs based on the shape of the signals, the cycles were first normalised using the percentile method. Then, shape-related features were extracted from each normalised cycle and used as input variables to build an automatic classifier algorithm based on Support Vector Machine (SVM), as reported previously [19,20]. For each sensing material, the classifier was used to make predictions of the VOC identification. The performance of the classifier was represented in confusion matrices, which show the rate of correct and incorrect predictions. The VOC identification ability of each sensor was given by the rate of correct predictions for that VOC.

Table 1

Composition of fibroin ionogels. *Water content measured by Karl Fischer titration.

Ionic Liquid	Structure	Fibroin Ionogel	Fibroin (% w/w)	Ionic liquid (% w/w)	Water added (% w/w)	Water in the IL (%)*
C ₂ mimCl	 Cl [⊖]	C ₂ F	8.3	91.7	0	1.72 ± 0.23
C ₆ mimCl	 Cl [⊖]	C ₆ F	8.8	91.2	0	1.17 ± 0.32
C ₁₀ mimCl	 Cl [⊖]	C ₁₀ F	6.4	87.9	6.07	0.79 ± 0.21

3. Results and discussion

3.1. Morphology and structure of fibroin ionogels in methylimidazolium chloride ionic liquids

Reconstituted silk fibroin presents the repeating motif Gly-Ala-Gly-Ala-Gly-Ser which typically assembles as anti-parallel β -sheets. This arrangement is maintained by the packing of short amino acid side chains of Gly and Ala in hydrophobic crystalline regions. In addition, extensive

intra- and inter-molecular hydrogen bond networks between N-H...O=C from neighbour backbone strands and between Ser OH groups and backbone O=C groups are important for the packing [21]. In the present work, lyophilised regenerated fibroin was used as the starting material in order to meet the challenge of producing fibroin ionogels with the lowest possible water content, as opposed to hybrid gels with 50% w/w of water as previously reported [11]. When the aqueous solution containing regenerated fibroin is lyophilised, there is a slight modification of the fibroin secondary structure, namely a decrease in random coil and small

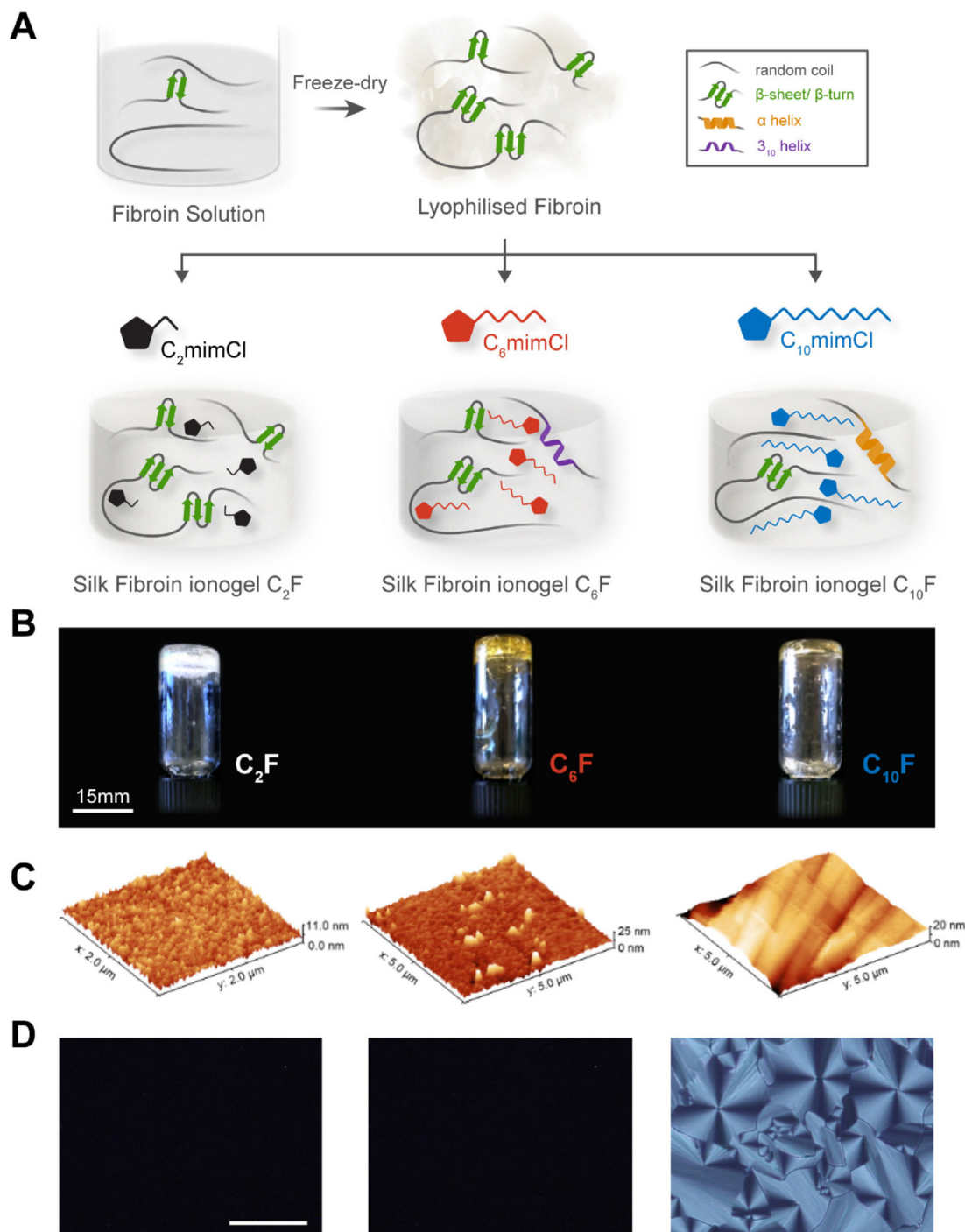


Fig. 1. Fibroin ionogels. (A) Schematic representation of fibroin ionogels and proposed predominant secondary structures. After dissolution of lyophilised fibroin and gelation in C_2 , C_6 and C_{10} mimCl ionic liquids, different fibroin secondary structures are observed. Scales are exaggerated for clarification. (B) Inverted glass vials containing fibroin ionogels. (C) Atomic Force Microscopy (AFM) topography and (D) Polarised Optical Microscopy (POM) taken with crossed polarisers at 90° of fibroin ionogels. The white line corresponds to 100 μm .

increase in β -sheet contents, rendering the final lyophilised fibroin sample water insoluble (Fig.S1 and Table S2 in Supplementary Information). The concept here explored involves the dissolution and gelation of the lyophilised silk fibroin sample in ILs, which represents a different challenge from most reports in which the ILs were used for dissolution and regeneration. The ILs need thus to disrupt the naturally occurring H-bonded network of fibroin, to further allow the formation of other networks of non-covalent interactions between silk fibroin chains and the ILs, giving rise to a physical gel.

The identity of both cation and anion IL moieties are important to promote the solubility of polymers in ILs, although it is known that the anion has a much larger effect on this process. Methylimidazolium-based ILs, with chloride as the anion, are known as the most successful for fibroin dissolution and regeneration [4], and were thus selected for this study. The chloride anion was selected due to its properties. It is a strong H-bond acceptor, known to break inter-strand hydrogen bonds between neighbour backbone polypeptide chains, thus critical for fibroin dissolution, but also able to act as a cross-linker in H-bonds, thus important for gel formation [22]. Regarding the cation moiety, we selected methylimidazolium cations with varying lengths of the alkyl chain, namely $C_n\text{mimCl}$ with $n = 2, 6, 10$. The alkyl chains will likely contribute for hydrophobic interactions, with the potential to disturb the closely packed hydrophobic pockets during fibroin dissolution but also to promote the formation of hydrophobic patches during gel assembly.

The selected methylimidazolium chloride ILs dissolved the lyophilised fibroin at high temperature. Upon cooling, we observed the formation of fibroin ionogels at 100, 100 and 70 mg mL^{-1} of fibroin for ILs C_2 , C_6 and $C_{10}\text{mimCl}$ (Fig. 1), respectively, while the control fibroin hydrogel was formed at lower concentration (50 mg mL^{-1} of fibroin) (Fig. S2). Remarkably, the water content of the fibroin ionogels was minimal, between 1 and 7% w/w, mostly attributable to the water already associated to the ILs used (Table 1). It was necessary to add a small amount of water to the fibroin ionogels produced with $C_{10}\text{mimCl}$ due to the initial low hydration content of the IL. The residual amount of water molecules existent in the final fibroin ionogel materials can contribute to H-bond formation, although the effect should be negligible considering the high IL content (higher than 88% w/w). It should be noted that the fibroin ionogels and controls were produced and then stored for 24 h at room temperature and controlled humidity (RH of 50%) before any characterizations or use. Apart from the detailed analysis that will follow for fibroin ionogels formed with $C_n\text{mimCl}$ ILs with $n = 2, 6$ and 10 , the mid-term alkyl chains $n = 4$ and $n = 8$ were also preliminarily assessed, to conclude that silk fibroin could also gelate C_4 and $C_8\text{mimCl}$ obtaining self-supporting ionogels similar to C_2 and $C_{10}\text{mimCl}$, respectively (Fig. S3).

The differences between the silk fibroin ionogels $C_2\text{F}$, $C_6\text{F}$ and $C_{10}\text{F}$ containing the ILs $C_2\text{mimCl}$, $C_6\text{mimCl}$ and $C_{10}\text{mimCl}$, respectively, were clear upon morphological characterisation by atomic force microscopy (AFM) and polarised optical microscopy (POM) under crossed polarisers (Fig. 1). The fibroin ionogel $C_2\text{F}$, containing the imidazolium IL with the shortest alkyl chain, was opaque, similar to the control hydrogel, which similar morphology was also proven by TEM imaging (Fig. S4). $C_2\text{F}$ ionogels presented small aggregates at the surface with RMS roughness of 1.1 nm, whereas fibroin hydrogel also presented aggregates, although larger, with RMS roughness of 5.2 nm (Fig. 1 and Fig. S2). Both $C_6\text{F}$ and $C_{10}\text{F}$ ionogels were translucent materials (the slight yellow coloration arises from the ionic liquid itself). The $C_6\text{F}$ ionogel presented dense and less homogeneous background with rodlike structures with increased roughness (2.4 nm RMS) when compared to $C_2\text{F}$ (Fig. 1). The $C_{10}\text{F}$ ionogel exhibited a distinct surface topography of aligned stripes, with a RMS roughness of 3.1 nm and unique birefringence showing a fan-like texture ascribed to the hexagonal liquid crystal phase by POM analysis (Fig. 1). This behaviour arises mostly from the self-assembling properties and molecular order of the IL used, $C_{10}\text{mimCl}$ [23], as described below.

To assess the contribution of the IL intrinsic self-assembling properties on the final silk fibroin ionogels, the three ILs were subjected to the

same processing steps as the fibroin ionogels. The heated/cooled IL controls ($C_2\text{HC}$ and $C_6\text{HC}$) formed viscous solutions (Fig. S5, Supplementary Information), showing that the presence of silk fibroin is essential for gel formation, except for $C_{10}\text{HC}$ which forms a self-supporting gel on its own. Imidazolium ILs with long alkyl chains have been reported to form lyotropic liquid crystal phases in the presence of water, due to their amphiphilic nature [23–25]. In particular, $C_{10}\text{mimCl}$ is reported to present unique self-assembly characteristics [23]. Moreover, a water content above 3% w/w can promote a H-bonded network and liquid crystalline gel phase with $C_{10}\text{mimCl}$ [26], which is the case in our work (water content 6.9% w/w). The $C_{10}\text{HC}$ gel presented a surface topography of stripes but with a higher RMS roughness (3.2 nm) when compared to $C_{10}\text{F}$. These results suggest that the IL self-assembling properties are predominant in the final hierarchical order of the fibroin ionogel, and that fibroin affects the organization of the IL creating smaller ordered clusters, suggesting that fibroin chains are interspersed in the IL supramolecular assemblies. A detailed investigation of the POM images obtained for the heat/cooled IL ($C_{10}\text{HC}$) and corresponding fibroin ionogel ($C_{10}\text{F}$) (Figs. S6 and S7) confirmed that both materials showed a fan-shaped pattern ascribed to the hexagonal liquid crystal phase, even though a decrease in the size of the fan-shaped structures was observed in the $C_{10}\text{F}$ fibroin ionogel. The hexagonal phase was recovered upon a heat-cool cycle in which the hexagonal-to-isotropic transition and reverse transition temperatures were similar.

The mechanical properties of silk fibroin ionogels and controls were assessed by dynamic frequency sweep measurements (Fig. 2A–B and Table S3 from Supplementary Information), after choosing a strain at the linear viscoelastic region from amplitude sweeps (Fig. S8 as an example). The $C_2\text{F}$ and $C_{10}\text{F}$ ionogels present viscoelastic behaviour as G' (10^4 and 10^6 Pa, respectively) is one order of magnitude greater than G'' . The $C_6\text{F}$ ionogel is the weakest, presenting G' and G'' in the 10^3 Pa order. The control $C_{10}\text{HC}$ also became stronger upon stress application and showed high moduli, but the storage and loss moduli are in the same order of magnitude (10^5 Pa), indicating that the presence of fibroin is key to enhance its viscoelasticity. From all tested materials, $C_{10}\text{F}$ ionogel presented the better mechanical robustness with G' of 1.3×10^6 Pa and G'' of 1.4×10^5 Pa.

The ATR-FTIR spectra of the fibroin ionogels tested (using each IL as background) helps to understand how silk fibroin chains could be organised within the gels (Fig. 2C–D). Comparing the spectra from lyophilised fibroin, control fibroin hydrogel and fibroin ionogels, it is possible to observe differences at important amide bands (Fig. S1, Table S2 and Fig. S9 Supplementary Information). For all the fibroin ionogels tested, the peak at the amide I region was shifted to a higher wavenumber (around 1660 cm^{-1}) when compared to the starting material (1624.69 cm^{-1}), suggesting alterations in secondary structure [27]. In turn, the amide II region ($1470\text{--}1570 \text{ cm}^{-1}$) shows a broader appearance, with more than one peak, which was already observable in the lyophilised fibroin. The amide III band ($1200\text{--}1350 \text{ cm}^{-1}$) presents broader peaks at the same wavenumbers as the fibroin hydrogel, which in turn points to β -sheets. In addition, the specific band at 1700 cm^{-1} , only visible in the control fibroin hydrogel, is stated as indicative of the antiparallel arrangement of fibroin chains in the β -sheet domains [28, 29]. The deconvolution of peaks at the amide I region ($1575\text{--}1800 \text{ cm}^{-1}$) indicates the most prevalent fibroin secondary structure in the different materials (Table S4), suggesting the existence of β -sheet (83%) and β -turn (17%) in the control fibroin hydrogel (as expected), and predominant β -turn (66%) and β -sheet (33%) in $C_2\text{F}$. In turn, $C_6\text{F}$ shows the presence of 3_{10} helix (63%), which can be also attributed to β -turns, in the addition to the 3% of attributable β -turns, and 33% of other conformations. Finally, $C_{10}\text{F}$ presents a strong presence of α -helix (79%), and the existence of β -turn (12%) and other (9%).

The materials were also characterized by X-ray scattering. As expected, the commercial fibroin solution showed an amorphous pattern, while the hydrogel presented one peak (2θ angles 23° (Fig. 2E and Fig. S10)), and a sharp ring at 4.32 \AA (Fig. 2F), which probably corresponds to

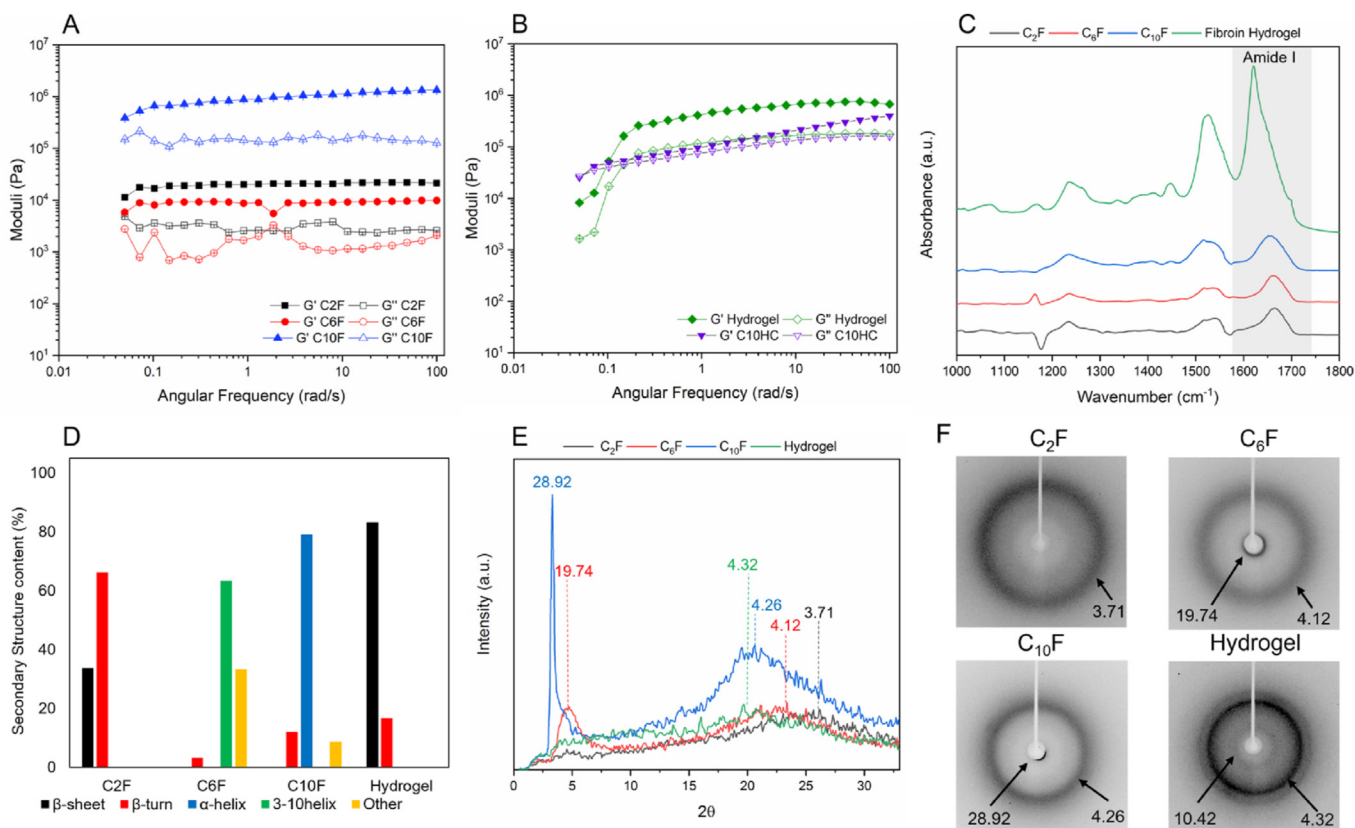


Fig. 2. Mechanical and structural characterisation of fibroin ionogels. (A) Rheology Frequency sweep measurements of fibroin ionogels C₂F, C₆F and C₁₀F. (B) Rheology Frequency sweep measurements of fibroin hydrogel and heat/cooled C₁₀HC. (C) ATR-FTIR spectra (Amide region) of fibroin ionogels C₂F, C₆F and C₁₀F, using the heat/cooled ILs as background, and compared with fibroin hydrogel, highlighting the Amide I band. (D) Secondary structure content from deconvolution of peaks at the Amide I band of ATR-FTIR spectra for each of the samples. (E) X-ray scattering 2θ scans of fibroin ionogels C₂F, C₆F, C₁₀F and fibroin hydrogel, with distances in Å annotated on top, and (F) taken from scattering ring intensity analysis.

a β -sheet crystalline periodic spacing. These results corroborate ATR-FTIR observations (Table S2), with the amorphous silk fibroin solution silk I re-organising into a more crystalline silk II structure upon mechanical stirring (hydrogel) or lyophilisation [6,30]. The two-dimensional scattering images acquired for the fibroin ionogels showed the presence of diffraction rings around 4 Å (wide angle region) which corresponds to a 2θ angle of around 22°. These diffraction rings were more diffused and less sharp than those observed for the control hydrogel which indicates more scattering and less ordered structures in the fibroin ionogels (Fig. 2E–F or Fig. S11). It is evident that the spacing corresponding to this scattering ring increases in value as the alkyl chain of the IL increases, visible at 3.71, 4.12 and 4.26 Å for C₂F, C₆F and C₁₀F, respectively. The value observable for C₁₀F approaches the 4.32 Å distance in the control hydrogel. It has been previously reported that attractive van der Waals interactions increase with increasing alkyl chain length on the cation C_nmim of the IL, which starts exhibiting amphiphilic character from $n = 10$ [24], and ultimately leads to an increase in order and crystal stabilisation [31]. For the C₆F ionogel, a second scattering ring is present in the small angle area, yielding a spacing value of 19.74 Å. The C₁₀F ionogels exhibit also a sharp scattering in the small angle albeit partially covered by the beamstop, which corresponds to a distance of 28.9 Å (Fig. 2E–F). X-ray scattering studies of pure ILs after undergoing a heat/cool cycle (labelled C_nHC) showed similar scattering patterns as to the corresponding fibroin ionogels (Fig. S11–S12). Still, the wide-angle region ring shifts to lower spacing in the fibroin ionogels, which points to more compact structures when fibroin is present.

The ILs selected for this study provide a multitude of interactions through the rich chemical diversity of cations and anions. When fibroin is dissolved in ILs, the intra- and inter-molecular H-bonds and hydrophobic

interactions between fibroin polypeptide chains are reduced, which, after cooling down, enable the formation of thermodynamically stable ionogels that do not exactly follow the typical secondary structure and supramolecular assembly of fibroin hydrogels.

The chloride anion is constant among all tested ILs. This anion is hydrophilic and a strong hydrogen bond acceptor [22], that can undertake multiple H-bonding interactions as doubly ionic [32] which act as a cross-linker between neighbour polypeptide chains. Regarding the cation moiety, the imidazolium ring is constant. Given the amino acid sequence of silk fibroin, it is expected that this ring mostly contributes as a weak hydrogen bond donor forming hydrogen bonds with hydrogen bond acceptor groups in the protein backbone and Ser side chain. But the most important contribution from the cation moiety is attributable to the alkyl chain that ranges from 2 to 10 carbons. The alkyl chain likely establishes hydrophobic interactions with the hydrophobic side chains of the fibroin, having an important role during dissolution and gelation. Particularly in gelation, the shortest alkyl chain seems to interfere less with fibroin assembly into β -sheets (according to ATR-FTIR) by possibly having little disruption on the hydrophobic packing of fibroin strands. The C₆F appears as the most disordered material, with less mechanical robustness and with the lack of predominant fibroin secondary structure. In C₁₀F we observe a synergistic effect between the strong self-assembling properties of the IL - which alone gives rise to a lyotropic liquid crystalline phase - and the physico-chemical properties of fibroin. After IL dissolution, the latter is forced to acquire a distinct secondary structure, rich in α -helix and β -turns, affecting the organization of the IL itself by creating smaller ordered clusters but still giving rise to birefringent and viscoelastic gels with higher G' than the control hydrogel and the heat/cooled IL.

3.2. Stability and ionic conductivity of fibroin ionogels

Fibroin ionogels acquire interesting properties due to the high content of ionic liquid, namely air and thermal stability, and high ionic conductivity. Analysis of the ionogels' stability upon storage at ambient conditions, as well as thermal assays, were carried out. When the gels are stored in an open vial at controlled humidity and temperature, the fibroin ionogels adsorb water from the atmosphere, reaching a maximum weight gain of 25, 16 and 10% w/w for C₂F, C₆F and C₁₀F, respectively, after 30 days of study. This is contrary to the behaviour of the hydrogel, which loses almost 60% of weight by drying out after 30 days (Fig. 3A–B). Yao and partners have shown that fibroin/C₂mimAcetate/H₂O gel almost maintains the original size and shape after exposed to air for 20 days [11], even though they have a 40–50% weight loss. That corresponds to the unbound water, as these gels were composed of 10% fibroin, 40% C₂mimAc and 50% water w/w [11]. In our work, fibroin ionogels present less than 27% water in their air-equilibrated composition after 30 days of air-storage (see insert of Fig. 3A). Such behaviour is likely attributable to the high hygroscopy of the ILs containing the chloride anion [22]. While C₆F and C₁₀F remain gels that can be handled with tweezers after 30 days, C₂F turned into a liquid state after 1 day of exposure to ambient air, likely due to the low self-assembling propensity of the IL alone. The heat/cooled ILs also gained weight throughout the storage time. It should

be noted that C₁₀HC remained a self-supporting gel after 30 days (Fig. S13A–B).

When comparing the mass loss curves from thermogravimetric analysis, it is clear that fibroin ionogels present larger thermal stability than the fibroin hydrogel, which loses mass abruptly until 150 °C (Fig. 3C). Fibroin ionogels lose mass almost entirely at 300 °C (as observed for the control heat/cooled ionic liquids, Fig. S14), as opposed to the 60% mass loss for the hydrogel for the same temperature, as previously reported [9]. Analysing the DSC scans, all fibroin ionogels present an endothermic peak between 77 and 110 °C (Fig. S15A), which represents the gel-sol transition. This is due to the reversible supramolecular gel formation that is based on weak physical forces such as H-bonding and van der Waals interactions [33]. The absence of a glass transition endotherm suggests that the materials are not completely amorphous [33], even though the X-ray scattering broad peaks point to no ordered structure within the ionogels. When compared to fibroin hydrogel (Fig. S16C), the fibroin ionogels present a larger degradation temperature, in addition to much larger enthalpies (T_D and ΔH_D in Fig. S15B), which means they require higher temperature and energy to degrade. This increasing thermal stability can be explained by decreasing Coulomb attraction if ideal ionic interaction is assumed, when opposed to hydrogels, where ionic interactions are not relevant [34]. The exothermic peak at ~100 °C for the hydrogel, as well as for the fibroin solution (see more detail in

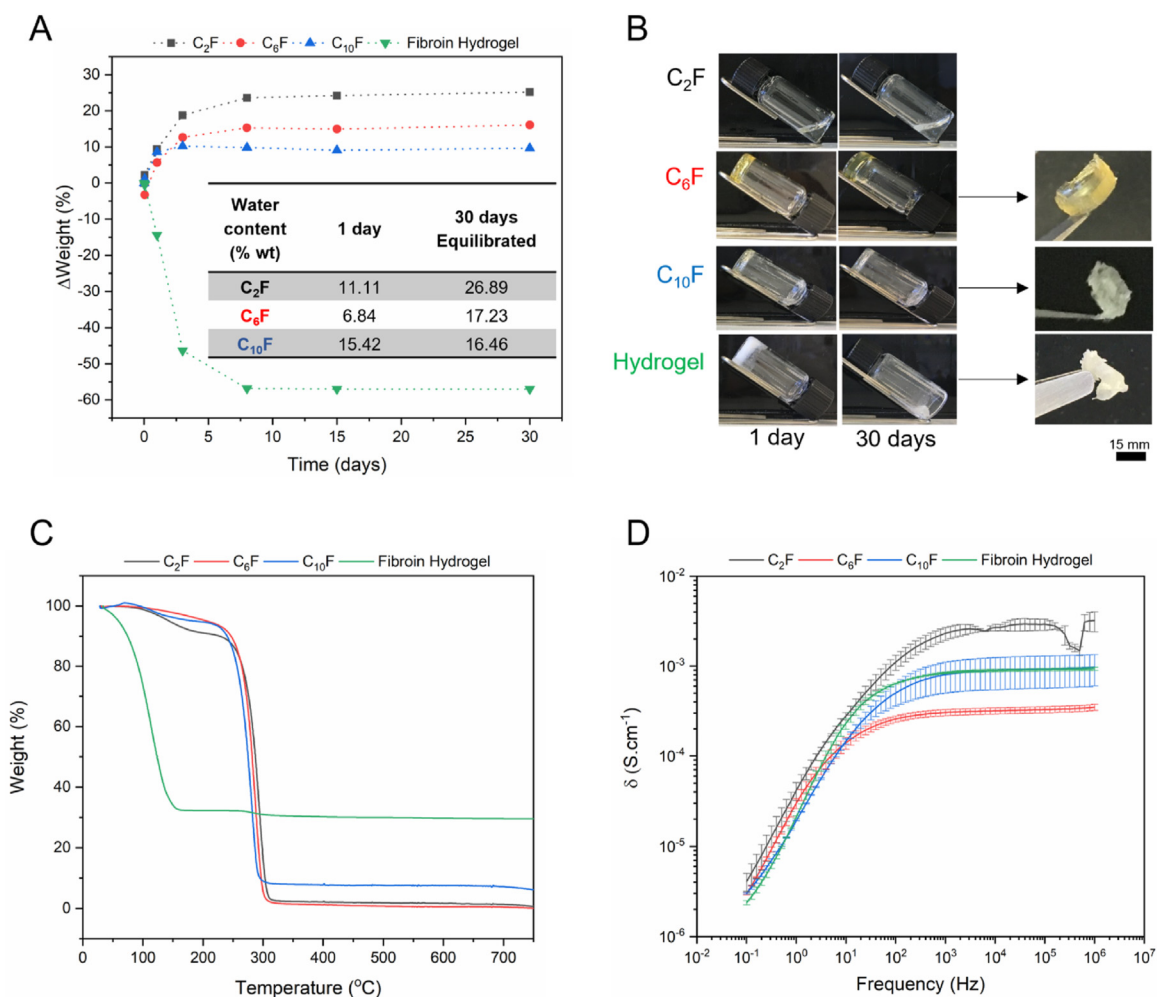


Fig. 3. Stability to air and temperature and ionic conductivity of fibroin ionogels. Stability study of fibroin ionogels C₂F, C₆F and C₁₀F versus fibroin hydrogel throughout time, upon storage of the open vials at ambient conditions ($T \approx 20$ °C; $RH \approx 50\%$). (A) Weight variance throughout storage time, comparing the mass at each time with the initial mass; Water content after 1 day and 30 days – equilibrated samples in the inset. (B) Macroscopic aspect of the gels after storage for 1 and 30 days, including when picked with the tweezers. (C) TGA analysis of fibroin ionogels versus hydrogel when heating the fibroin ionogels and hydrogel at 10 °C/min. (D) Ionic conductivity spectra of fibroin iono- and hydrogels at ambient conditions.

Fig. S16B) coincide with the TGA weight loss at this temperature range (Fig. S16A), just before the glass transition (T_G values of 120 and 112 °C, respectively, as seen in Fig. S16C). The crystallisation of fibroin induced by heat was above 250 °C for all the fibroin materials (exothermic peak), as previously reported [35]. In addition, the following degradation temperatures (T_D at which Δ_{max} is achieved) increase when there is less water (Fig. S16C). As opposed to amorphous silk fibroin, for which the decomposition has been reported by some researchers to occur at $T < 290$ °C [28,36], the analysed fibroin ionogels showed decomposition peaks at larger temperatures (T_D) (Fig. S15B) – with the exception of C₆F. The degree of molecular orientation and crystallinity, that give the morphological and physical properties to the sample, are the main responsible factors for this thermal behaviour [29], which actually confirms the morphological, mechanical and structural analysis (Fig. 2).

Intrinsic ionic conductivity of the fibroin ionogels is another unique characteristic endowed by the high IL content. The ionogels' ionic conductivity is attributed to the mobility of the ILs cations and anions within the gels. The fibroin hydrogel also presented ionic conductivity (Fig. 3D),

very similar to the one found for C₁₀F ionogel due to the presence of water. All ionogels, except C₆F, presented a maximum ionic conductivity in the range of 10^{-3} - 10^{-2} S cm⁻¹, which is above the benchmark of 1 mS cm⁻¹ required in electrochemical devices [37]. It has been reported that increased IL content or decreased silk fibroin content can raise the ionic conductivity [11]. In this work, the conductivities achieved for C₂HC and C₁₀HC were similar to their corresponding fibroin ionogels C₂F and C₁₀F, with the large error bars from duplicates actually pointing to a larger variability of the controls (Fig. S17), indicating the stabilising effect of fibroin polypeptide chains. As already expected [38], an increase in the alkyl chain length of the imidazolium cation lowered the ionic conductivity, with C₂F presenting the largest ionic conductivity. However, the C₆F showed lower conductivity than C₁₀F, which could be explained by the less organised structures within the C₆F gel, lowering ion mobility. Even though C₂F ionogel presents the highest conductivity, it has the lowest air-stability with C₁₀F having the best compromise between conductivity and air stability.

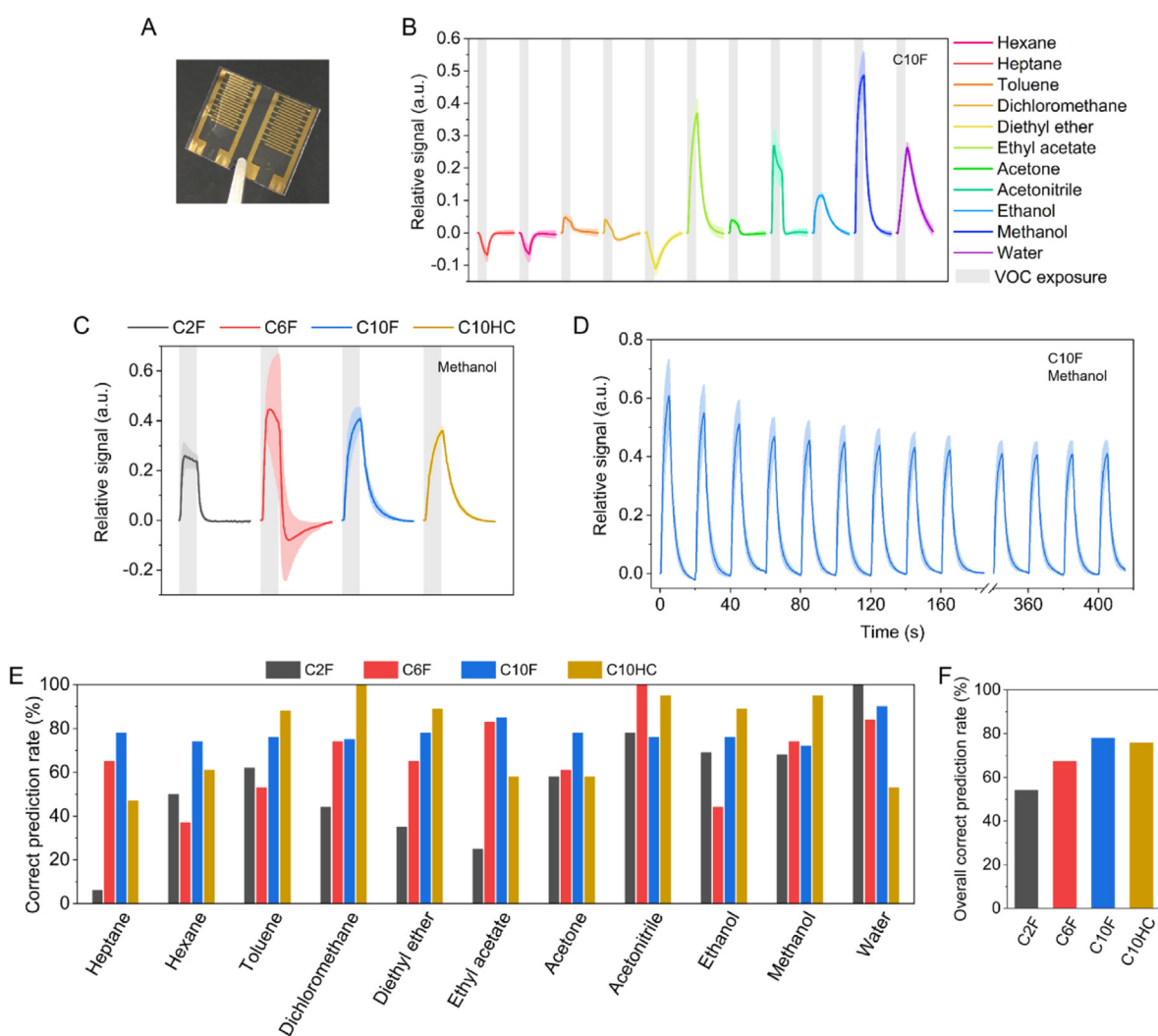


Fig. 4. Application of fibroin ionogels in gas sensing. VOC sensing experiment using the in-house developed electronic nose. (A) Macroscopic aspect of C₁₀F films spread on top of a glass slide patterned with interdigitated gold electrodes after used on the electronic nose. (B) Typical cycle signals of a C₁₀F sensor upon exposure to different VOCs and water. Each curve represents the average and standard deviation of at least 19 replicate cycles from a same sensor. VOC exposure periods (5 s) are highlighted in grey. (C) Typical cycle signal of the sensors made of fibroin ionogels and heat/cooled ionic liquid C₁₀HC when exposed to methanol (5 s, highlighted in grey). The lines and shadow are the average signal and standard deviation of the 2 independent sensors. (D) Representation of all the cycles performed during the 7.5 min experiment with methanol when using 2 independent C₁₀F films as sensors. The line and shadow are the average signal and standard deviation of 2 independent sensors. (E) Comparison of correct VOC prediction rates obtained when using each fibroin ionogel and heat/cooled ionic liquid C₁₀HC as gas sensors. (F) Overall correct VOC prediction rate for each sensor, given by the average of the correct prediction rate of all the VOCs.

3.3. Fibroin ionogels as electrical gas sensors

The synergy between remarkable air-stability and high ionic conductivity of the fibroin ionogels was here combined to assess a potential application of the materials in the field of artificial olfaction.

After proving that fibroin ionogels present ionic conductivity, they were spread as thin films on top of interdigitated gold electrodes (Fig. 4A) and used as sensors in our in-house built electronic nose (set-up on Fig. S18). Due to the intrinsic ionic conductivity property of the ionogel material, when an alternate voltage is applied between the terminals of the interdigitated electrodes, it causes ions movement within the ionogel, generating an electrical current. Our electronic nose detects that current and converts it to a voltage value that is proportional to the conductance of the ionogel. This is the electrical signal of the material in rest. When we expose the ionogels to vapours of different chemicals or water vapour, we observe changes in their rest electrical signal, which represent changes in ionic movement within the ionogel caused by the interactions established between the incoming vapour molecules and the ionogel. Thus, our ionogels report the adsorption/desorption of gas molecules through the variation of their electrical signal, as shown in Fig. 4B and C. Even though the hydrogel showed a high ionic conductivity, it did not qualify as electrical gas sensor because it loses water by evaporation and a rigid dry material forms, preventing charges to move. In our VOC sensing experiment, the fibroin sensors' signals were recorded during 22 consecutive cycles of exposure to VOC (5 s) followed by ambient air (15 s) (for recovery of the baseline). Different VOCs have different characteristic signals for each sensor composition (Fig. 4B, for C₁₀F sensor), which is related with the distinct dynamics and types of interactions that occur during VOC adsorption/desorption to the ionogel. Also, signals are different for each sensor composition upon exposure to the same VOC (Fig. 4C, for methanol). For example, regarding exposure to methanol, C₂F returns relatively quickly (1.6 ± 0.4 s) to its initial conductance, while C₁₀F and C₁₀HC take longer (5.8 ± 1.6 s and 6.6 ± 0.8 s, respectively) to recover, resembling a more triangular-shape signal. As it is possible to observe from the 22 exposure/recovery cycles in Fig. 4D (example of C₁₀F response to methanol), the sensors were relatively stable throughout the 7.5 min experiment, yielding reversible and repeatable signals after the first 6 cycles. This corresponds to the sensor's stabilisation time of around 2 min (where the signal amplitude variability is 29%), after which the signal amplitude can be considered constant, with a variability lower than 4% for each independent sensor. From all the 10 VOCs tested, chloroform was the only one that clearly damaged films containing fibroin (with the exception of C₁₀mimCl-based thin films). The control C₁₀HC also presented deterioration after exposure to the tested VOCs, which was not observable for the C₁₀F sensor, indicating the important role of fibroin to maintain the integrity of the material.

After collecting signals from the sensors upon VOC exposure, we used an automatic classifier based on support vector machines (SVM) that analyses the cycles' shape. The cycles were normalised (see the mean normalised waves for each sensor in Figure S19-S22 of Supplementary Information), showing singular signatures for different VOC chemical classes and sensors. The rate of correct VOC predictions (%) was taken from the diagonal of each confusion matrix and presented in Fig. 4E (from Fig. S23). C₁₀F correctly identified all VOCs with an overall correct prediction rate higher than 80%, emerging as the most promising gas-sensing film allied to higher robustness.

In previous works, we reported similar gas-sensing gel materials, where an optical probe (liquid crystal) was added to the ionogel, resulting in hybrid gels that yield optical signals with different shapes for different VOCs [39] and have excellent VOC prediction ability (98.9% overall correct prediction rate [20]). Fibroin ionogel materials still present lower VOC prediction ability (around 80%, Fig. 4F) than the optical gelatin hybrid gels but are more robust mechanically and simpler to produce because less components are required than for gelatin hybrid gels. The combination of fibroin and C₁₀mimCl yielded gels with G' and G'' in the order of 10^6 and 10^5 , respectively, whereas the reported gelatin

ionogels have G' and G'' in the order of 10^3 and 10^1 , respectively [39]. The required signal acquisition hardware is simpler in the case of ionogels. The simplicity and improved mechanical properties might be favourable for several applications. Thus, the fibroin ionogel sensing system would benefit from further work to optimize the VOC prediction ability, namely by gathering a larger dataset of signals collected with C₁₀F sensors from different batches, providing a more accurate representation of the variability of the signal shape per VOC.

4. Conclusions

In summary, we explore the synergy between silk fibroin and ILs, through the dissolution and gelation of lyophilised fibroin in selected ILs, giving rise to fibroin ionogels with the lowest water content ever reported, and with unique properties that arise from the combination of both components. The fact that the fibroin polypeptide chains are dissolved in ILs and further allowed to reform thermodynamically stable structures in a high IL content, gave rise to physical ionogels with distinct properties largely dependent on the alkyl chain length moiety of the anion. In fact, the 1-alkyl-3-methylimidazolium chloride ILs act as designer solvents that can tune the induced fibroin secondary structures and the hierarchical organisation of the two components into physical gels. Even though the ILs with larger alkyl chain, such as C₁₀mimCl, are known to have their own assembly and crystalline tendency, fibroin enhances the ionogel's mechanical strength despite the absence of β -sheet arrangement, making C₁₀F the most stable to air and temperature. In turn, the presence of short alkyl chain length cations has little impact on the fibroin natural assembly, allowing for β -sheet structures to be reformed, which explains the greater mechanical properties of fibroin ionogel using C₂mimCl when compared to the one with C₆mimCl, and is also corroborated by the shorter spacings analysed from X-ray scattering patterns. Owing to the characteristics of ILs, the fibroin ionogels were shown not to evaporate and to possess high ionic conductivity, thus creating fibroin sensing layers, in which fibroin is not a passive substrate where active substances are introduced but fibroin is part of the active layer. It is thus possible to produce air-stable fibroin thin films that can be used as gas sensors, in contrary to the fibroin hydrogels that dry out, inhibiting charge mobility. This work sets the ground for establishing fibroin as a much versatile element in flexible and wearable bioelectronic devices.

Credit author statement

Inês Moreira: Investigation, Validation, Writing – original draft; Ana Luísa Carvalho: Investigation; Inês Moreira, Carina Esteves, Susana Palma and Efthymia Ramou: Formal analysis; Carina Esteves, Susana Palma and Efthymia Ramou: Writing – review & editing; Ana Roque: Conceptualization, Methodology, Resources, Supervision, Writing – review & editing.

Declaration of competing interest

The authors declare that they have no known competing financial interests or personal relationships that could have appeared to influence the work reported in this paper.

Acknowledgements

This project has received funding from the European Research Council (ERC) under the EU Horizon 2020 research and innovation programme (grant agreement No. SCENT-ERC-2014-STG-639123, 2015–2022) and by the national funds from Fundação para a Ciência e Tecnologia, I.P. (FCT), in the scope of the project PTDC/BII-BIO/28878/2017, PTDC/CTM-CTM/3389/2021, UIDP/04378/2020 and UIDB/04378/2020 of the Research Unit on Applied Molecular Biosciences - UCIBIO and the project LA/P/0140/2020 of the Associate Laboratory

Institute for Health and Bioeconomy - i4HB. Carina Esteves thanks FCT for the PhD grant SFRH/BD/113112/2015 and Ana Luísa Carvalho for grant RECI/BBB-BEP/0124/2014, which financed the X-ray Diffraction Facility of UCIBIO. The authors also thank Dr. Erin Tranfield and Sofia Pacheco from Instituto Gulbenkian da Ciência (IGC) for the TEM preparation and images, Prof. Isabel Ferreira and João Carmo from CEN-IMAT/I3N, for their help with the conductivity measurements and Prof. Ana Rita Duarte from Associate Laboratory for Green Chemistry – LAQV for facilitating the rheology equipment. We acknowledge Elisabete Ferreira and the Biolab services from UCIBIO for the lyophilisation. We also thank the LAQV analysis lab for the TGA/DSC and XRPD experiments. LA/P/0140/2020 and Associate Laboratory Institute for Health and Bioeconomy - i4HB, Portugal.

Appendix A. Supplementary data

Supplementary data to this article can be found online at <https://doi.org/10.1016/j.mtbio.2022.100290>.

References

- D.L. Wen, D.H. Sun, P. Huang, W. Huang, M. Su, Y. Wang, et al., Recent progress in silk fibroin-based flexible electronics, *Microsyst. Nanoeng.* 7 (2021), <https://doi.org/10.1038/s41378-021-00261-2>.
- B. Zhu, H. Wang, W.R. Leow, Y. Cai, X.J. Loh, M.Y. Han, et al., Silk fibroin for flexible electronic devices, *Adv. Mater.* 28 (2016) 4250–4265, <https://doi.org/10.1002/adma.201504276>.
- H.Y. Wang, Z.G. Wei, Y.Q. Zhang, Dissolution and regeneration of silk from silkworm *Bombyx mori* in ionic liquids and its application to medical biomaterials, *Int. J. Biol. Macromol.* 143 (2020) 594–601, <https://doi.org/10.1016/j.ijbiomac.2019.12.066>.
- D.M. Phillips, L.F. Drummy, D.G. Conrady, D.M. Fox, R.R. Naik, M.O. Stone, et al., Dissolution and regeneration of *Bombyx mori* silk fibroin using ionic liquids, *J. Am. Chem. Soc.* 126 (2004) 14350–14351, <https://doi.org/10.1021/ja046079f>.
- T. Asakura, A. Kuzuhara, R. Tabeta, H. Saito, Conformation characterization of *Bombyx mori* silk fibroin in the solid state by high-frequency ¹³C cross polarization-magic angle spinning NMR, X-ray diffraction, and infrared spectroscopy, *Macromolecules* 18 (1985) 1841–1845, <https://doi.org/10.1021/ma00152a009>.
- D.M. Phillips, L.F. Drummy, R.R. Naik, H.C. De Long, D.M. Fox, P.C. Trulove, et al., Regenerated silk fiber wet spinning from an ionic liquid solution, *J. Mater. Chem.* 15 (2005) 4206–4208, <https://doi.org/10.1039/b510069k>.
- N. Goujon, X. Wang, R. Rajkova, N. Byrne, Regenerated silk fibroin using protic ionic liquids solvents: towards an all-ionic-liquid process for producing silk with tunable properties, *Chem. Commun.* 48 (2012) 1278–1280, <https://doi.org/10.1039/c2cc17143k>.
- S.S. Silva, E.G. Popa, M.E. Gomes, M.B. Oliveira, S. Nayak, B. Subia, et al., Silk hydrogels from non-mulberry and mulberry silkworm cocoons processed with ionic liquids, *Acta Biomater.* 9 (2013) 8972–8982, <https://doi.org/10.1016/j.actbio.2013.06.044>.
- J. Stanton, Y. Xue, P. Pandher, L. Malek, T. Brown, X. Hu, et al., Impact of ionic liquid type on the structure, morphology and properties of silk-cellulose biocomposite materials, *Int. J. Biol. Macromol.* 108 (2018) 333–341, <https://doi.org/10.1016/j.ijbiomac.2017.11.137>.
- A. Reizabal, D.M. Correia, C.M. Costa, L. Perez-Alvarez, J.L. Vilas-Vilela, S. Lanceros-Méndez, Silk fibroin bending actuators as an approach toward natural polymer based active materials, *ACS Appl. Mater. Interfaces* 11 (2019) 30197–30206, <https://doi.org/10.1021/acsami.9b07533>.
- M. Yao, D. Su, W. Wang, X. Chen, Z. Shao, Fabrication of air-stable and conductive silk fibroin gels, *ACS Appl. Mater. Interfaces* 10 (2018) 38466–38475, <https://doi.org/10.1021/acsami.8b14521>.
- E. Andrzejewska, A. Marcinkowska, A. Zgrzeba, Ionogels - materials containing immobilized ionic liquids, *Polimery/Polymers* 62 (2017) 344–352, <https://doi.org/10.14314/polimery.2017.344>.
- L. Liu, Y. Han, S. Lv, Design of self-healing and electrically conductive silk fibroin-based hydrogels, *ACS Appl. Mater. Interfaces* 11 (2019) 20394–20403, <https://doi.org/10.1021/acsami.9b04871>.
- X. Liu, J. Liu, J. Wang, T. Wang, Y. Jiang, J. Hu, et al., Bioinspired, microstructured silk fibroin adhesives for flexible skin sensors, *ACS Appl. Mater. Interfaces* 12 (2020) 5601–5609, <https://doi.org/10.1021/acsami.9b21197>.
- A. Reizabal, S. Gonçalves, N. Pereira, C.M. Costa, L. Pérez, J.L. Vilas-Vilela, et al., Optically transparent silk fibroin/silver nanowire composites for piezoresistive sensing and object recognitions, *J. Mater. Chem. C* 8 (2020) 13053–13062, <https://doi.org/10.1039/d0tc03428b>.
- R. Ranjana, N. Parushuram, K.S. Harisha, S. Asha, B. Narayana, M. Mahendra, et al., Fabrication and characterization of conductive silk fibroin–gold nanocomposite films, *J. Mater. Sci. Mater. Electron.* 31 (2020) 249–264, <https://doi.org/10.1007/s10854-019-02485-5>.
- Q. Liu, S. Yang, J. Ren, S. Ling, Flame-retardant and sustainable silk ionotropic skin for fire alarm systems, *ACS Mater. Lett.* 2 (2020) 712–720, <https://doi.org/10.1021/acsmaterlett.0c00062>.
- R.T. Da Rocha, I.G.R. Gutz, C.L. Do Lago, A low-cost and high-performance conductivity meter, *J. Chem. Educ.* 74 (1997) 572–574, <https://doi.org/10.1021/ed074p572>.
- G. Santos, C. Alves, A.C. Pádua, S. Palma, H. Gamboa, A.C. Roque, An optimized E-nose for efficient volatile sensing and discrimination, in: *Proc 12th Int Jt Conf Biomed Eng Syst Technol (BIOSTEC)*, 2019, pp. 36–46, 2019.
- C. Esteves, G.M.C. Santos, C. Alves, S.I.C.J. Palma, A.R. Porteira, J. Filho, et al., Effect of film thickness in gelatin hybrid gels for artificial olfaction, *Mater. Today Bio* 1 (2019) 100002, <https://doi.org/10.1016/j.mtbio.2019.100002>.
- Y. Wang, B.J. Kim, W. Li, M. Li, Controlling silk fibroin conformation for dynamic, responsive, multifunctional, micropatterned surfaces, *Proc. Natl. Acad. Sci. Unit. States Am.* 116 (2019) 21361–21368, <https://doi.org/10.1073/pnas.1911563116>.
- C. Esteves, S.I.C.J. Palma, H.M.A. Costa, C. Alves, G.M.C. Santos, E. Ramou, et al., Tackling humidity with designer ionic liquid-based gas sensing soft materials, *Adv. Mater.* 34 (2022), <https://doi.org/10.1002/adma.202107205>.
- S. Saouane, F.P.A. Fabbiani, Structural behavior of long-chain imidazolium-based ionic liquid [C10mim]Cl-water mixtures, *Cryst. Growth Des.* 15 (2015) 3875–3884, <https://doi.org/10.1021/acs.cgd.5b00494>.
- J.D. Holbrey, K.R. Seddon, The phase behaviour of 1-alkyl-3-methylimidazolium tetrafluoroborates; ionic liquids and ionic liquid crystals, *J. Chem. Soc., Dalton Trans.* (1999) 2133–2139, <https://doi.org/10.1039/a902818h>, 0.
- T. Inoue, B. Dong, L.Q. Zheng, Phase behavior of binary mixture of 1-dodecyl-3-methylimidazolium bromide and water revealed by differential scanning calorimetry and polarized optical microscopy, *J. Colloid Interface Sci.* 307 (2007) 578–581, <https://doi.org/10.1016/j.jcis.2006.12.063>.
- J. Kusteklis, V. Balevičius, V. Aleksa, Two-dimensional Raman spectroscopy study of ionogel phase formation in long-chain ionic liquid/water systems, *J. Raman Spectrosc.* 48 (2017) 126–131, <https://doi.org/10.1002/jrs.4983>.
- E. Kamalha, Y.S. Zheng, Y.C. Zeng, M.N. Fredrick, FTIR and WAXD study of regenerated silk fibroin, *Adv. Mater. Res.* 677 (2013) 211–215, <https://doi.org/10.4028/www.scientific.net/amr.677.211>.
- G.M. Nogueira, A.C.D. Rodas, C.A.P. Leite, C. Giles, O.Z. Higa, B. Polakiewicz, et al., Preparation and characterization of ethanol-treated silk fibroin dense membranes for biomaterials application using waste silk fibers as raw material, *Bioresour. Technol.* 101 (2010) 8446–8451, <https://doi.org/10.1016/j.biortech.2010.06.064>.
- M. Tsukada, M. Obo, H. Kato, G. Freddi, F. Zanetti, Structure and dyeability of *Bombyx mori* silk fibers with different filament sizes, *J. Appl. Polym. Sci.* 60 (1996) 1619–1627, [https://doi.org/10.1002/\(SICI\)1097-4628\(199606\)60:10<1619::AID-APP14>3.0.CO;2-#](https://doi.org/10.1002/(SICI)1097-4628(199606)60:10<1619::AID-APP14>3.0.CO;2-#).
- Q. Lv, C. Cao, H. Zhu, Clotting times and tensile properties of insoluble silk fibroin films containing heparin, *Polym. Int.* 54 (2005) 1076–1081, <https://doi.org/10.1002/pi.1814>.
- J.D. Holbrey, W.M. Reichert, M. Nieuwenhuysen, S. Johnston, K.R. Seddon, R.D. Rogers, Crystal polymorphism in 1-butyl-3-methylimidazolium halides: supporting ionic liquid formation by inhibition of crystallization, *Chem. Commun.* 9 (2003) 1636–1637, <https://doi.org/10.1039/b304543a>.
- P.A. Hunt, C.R. Ashworth, R.P. Matthews, Hydrogen bonding in ionic liquids, *Chem. Soc. Rev.* 44 (2015) 1257–1288, <https://doi.org/10.1039/c4cs00278d>.
- P. Mcneice, Y. Zhao, J. Wang, G.F. Donnelly, P. Marr, Low molecular weight gelators (LMWGs) for ionic liquids: the role of hydrogen bonding and sterics in the formation of stable low molecular weight ionic liquid gels, *Green Chem.* 19 (2017) 4690–4697, <https://doi.org/10.1039/c7gc02053h>.
- A. Efimova, G. Hubrig, P. Schmidt, Thermal stability and crystallization behavior of imidazolium halide ionic liquids, *Thermochim. Acta* 573 (2013) 162–169, <https://doi.org/10.1016/j.tca.2013.09.023>.
- S.W. Ha, Y.H. Park, S.M. Hudson, Dissolution of *bombyx mori* silk fibroin in the calcium nitrate tetrahydrate-methanol system and aspects of wet spinning of fibroin solution, *Biomacromolecules* 4 (2003) 488–496, <https://doi.org/10.1021/bm0255948>.
- G. Freddi, G. Pessina, M. Tsukada, Swelling and dissolution of silk fibroin (*Bombyx mori*) in N-methyl morpholine N-oxide, *Int. J. Biol. Macromol.* 24 (1999) 251–263, [https://doi.org/10.1016/S0141-8130\(98\)00087-7](https://doi.org/10.1016/S0141-8130(98)00087-7).
- I. Stepniak, E. Andrzejewska, Highly conductive ionic liquid based ternary polymer electrolytes obtained by in situ photopolymerisation, *Electrochim. Acta* 54 (2009) 5660–5665, <https://doi.org/10.1016/j.electacta.2009.05.004>.
- J. Vila, L.M. Varela, O. Cabeza, Cation and anion sizes influence in the temperature dependence of the electrical conductivity in nine imidazolium based ionic liquids, *Electrochim. Acta* 52 (2007) 7413–7417, <https://doi.org/10.1016/j.electacta.2007.06.044>.
- A. Hussain, A.T.S. Semeano, S.I.C.J. Palma, A.S. Pina, J. Almeida, B.F. Medrado, et al., Tunable gas sensing gels by cooperative assembly, *Adv. Funct. Mater.* 1700803 (2017) 1–9, <https://doi.org/10.1002/adfm.201700803>.